PHYSICAL REVIEW E **76**, 041121 (2007)

Parameterization of the nonlocal viscosity kernel for an atomic fluid

J. S. Hansen[*]
Centre for Molecular Simulation, Swinburne University of Technology, P.O. Box 218, Hawthorn, Victoria 3122, Australia

Peter J. Daivis[†]
Applied Physics, School of Applied Sciences, RMIT University, G.P.O. Box 2476V, Melbourne, Victoria 3001, Australia

Karl P. Travis[‡]
Immobilisation Science Laboratory, Department of Engineering Materials, University of Sheffield, Mappin Street, Sheffield S1 3JD, United Kingdom

B. D. Todd[§]
Centre for Molecular Simulation, Swinburne University of Technology, P.O. Box 218, Hawthorn, Victoria 3122, Australia

(Received 15 June 2007; published 15 October 2007)

In this paper we present results for the wave-vector dependent shear viscosity for a model atomic fluid with short ranged repulsive interactions computed by molecular dynamics simulations. It is shown that the data can be fitted to two different simple functional forms over a large density range, namely, a function composed of two Gaussian terms and a Lorentzian type function with a variable wave-vector exponent. The parameters of both functional forms are found to obey simple density dependencies. While the first functional form has the advantage that the inverse Fourier transform can be found analytically, the Lorentzian type function fits the wave-vector dependence better over the range of wave vectors and densities studied here. The results show that the real space viscosity kernel has a width of 2 to 3 atomic diameters. This means that the generalized hydrodynamic constitutive relation is required if the strain rate varies significantly over this distance, a situation commonly encountered for nanofluidic flows.

DOI: 10.1103/PhysRevE.76.041121 PACS number(s): 05.20.Jj, 66.20.+d, 66.90.+r, 47.11.Mn

I. INTRODUCTION

It is well-known that Newton's law of viscosity breaks down when sufficiently large changes in the strain rate occur over a sufficiently small length scale, of the same order as the range of the intermolecular correlations [1–5]. The local viscosity defined by Newton's law even exhibits singularities at points where the strain rate is zero [3,4]. This means that the stress cannot be thought of as a local (or point) function of the strain rate. Therefore in the same way that every fluid must be regarded as viscoelastic, leading to a stress response that is nonlocal in time, the stress response of all fluids must also be regarded as being spatially nonlocal. In order to generalize the definition of the viscosity, Evans and Morriss [2], following the well-established ideas of generalized hydrodynamics [1,6,7] have proposed a nonlocal constitutive equation that allows for spatial and temporal nonlocality for a homogeneous fluid:

$$P_{xy}(\mathbf{r},t) = -\int_0^t \int_{-\infty}^{\infty} \eta(\mathbf{r}-\mathbf{r}',t-t')\dot{\gamma}(\mathbf{r}',t')d\mathbf{r}'dt', \quad (1)$$

where $P_{xy}(\mathbf{r},t)$ and $\dot{\gamma}(\mathbf{r},t)$ are the xy pressure tensor element and shear strain rate at position $\mathbf{r}$ and time t and $\eta(\mathbf{r}-\mathbf{r}, t-t')$ is the nonlocal viscosity kernel. In the situation where the strain rate is constant in time and only varies with respect to the spatial coordinate y, Eq. (1) can, in the case of a homogeneous fluid, be written as

$$P_{xy}(y) = -\int_{-\infty}^{\infty} \eta(y-y')\dot{\gamma}(y')dy'. \quad (2)$$

A constitutive equation of this form is expected to be necessary for the description of flow of a confined fluid, due to the large change in the strain rate with position in the vicinity of the walls [3]. Conversely, it might be expected that the viscosity kernel could be obtained by first determining the stress and strain rate in a fluid that is confined to a narrow channel and then solving Eq. (2). However, even if the stress and the strain rate in the fluid are known the integral equation cannot be readily solved. To our knowledge only Zhang *et al.* [4] have attempted to extract a viscosity kernel by this method. In their work a confined fluid was subjected to planar Poiseuille flow and they were able to obtain data for an effective nonlocal viscosity kernel by assuming that the viscosity kernel was independent of position, i.e., $\eta(y,y-y')=\eta(y-y')$. This assumption is only strictly valid for spatially homogeneous fluids, so this approach is ultimately unsuitable for application to confined fluids. Furthermore, since the data analysis for a bounded system involves inverse Fourier transforms of truncated data, undesirable technical difficulties arise [5,8].

An obvious alternative to direct inversion of stress-strain rate data for a bounded system is to determine the viscosity

---

[*] jhansen@ict.swin.edu.au
[†] peter.daivis@rmit.edu.au
[‡] k.travis@sheffield.ac.uk
[§] btodd@swin.edu.au

kernel independently for an unconfined, homogeneous fluid over an appropriate range of temperatures and densities and then use the constitutive equation [Eq. (2)] with appropriate boundary conditions to predict the flow profile for the confined fluid.

The aim of this work is to perform the first step in this process by extracting the exact homogeneous nonlocal viscosity kernel and parameterizing it in a form that is suitable for input into nanofluidic flow computations at the level of generalized hydrodynamics. We do this by performing extensive equilibrium (EMD) and homogeneous nonequilibrium molecular dynamics (NEMD) simulations. Since the domain is spatially homogeneous and since the data does not suffer from any truncation we overcome the problems faced previously. With the exact molecular dynamics results we wish to propose a satisfactory functional form for the nonlocal viscosity kernel in Fourier space that fits the data for a variety of state points which are found in a typical NEMD simulation of a confined fluid flow. This functional form must naturally have properties that allow an inverse transformation to the y-space viscosity kernel.

This paper is organized as follows: In Sec. II we describe the EMD and NEMD methods applied. In Sec. III we present the results and discuss the most applicable functional forms. In Sec. IV we draw our conclusions and make a few closing remarks.

II. METHODS

A. Equilibrium molecular dynamics

The zero shear rate limit of the wave-vector dependent viscosity can be calculated from the equilibrium correlation function of the transverse momentum density using well-known relationships derived from the theory of generalized hydrodynamics [1,2]. In principle, the wave-vector and frequency dependent viscosity could be computed from either the stress autocorrelation function or the transverse momentum density autocorrelation function [2]. In the case of the transverse momentum density autocorrelation function, if we form the correlation function of the fluctuations in fluid velocity in the x direction having a velocity gradient in the y direction, the appropriate relationship is

$$\eta(k_y,\omega)=\frac{C(k_y,t=0)-i\omega C(k_y,\omega)}{C(k_y,\omega)k^2\rho}, \tag{3}$$

where ρ is the number density of the fluid and $C(k_y,\omega)$ is the Laplace transform of the ensemble averaged transverse momentum density autocorrelation function $C(k_y,t)$ which is defined as

$$C(k_y,t)=\frac{1}{V}\langle J_x(k_y,t)J_x(-k_y,0)\rangle. \tag{4}$$

The transverse momentum density is defined in terms of the atomic positions and momenta as

$$J_x(k_y,t)=\sum_{i=1}^{N}p_{ix}e^{ik_yx_i}. \tag{5}$$

The zero time value of the canonical ensemble average of the transverse momentum density autocorrelation function in the thermodynamic limit is

$$C(k_y,t=0)=\rho k_BT. \tag{6}$$

In practice, the value of $C(k_y,t{=}0)$ obtained from simulation differs slightly from the exact value given by this equation due to finite time averaging and the finite system size, which results in corrections of order $(1/N)$. Therefore we use the simulated value of $C(k_y,t{=}0)$ in calculations to ensure numerical consistency of the computed properties.

The expression for the generalized shear viscosity in terms of the autocorrelation function of the shear stress is

$$\eta(k_y,\omega)=\frac{N(k_y,\omega)}{C(k_y,t=0)\rho k_BT-k^2N(k_y,\omega)i\omega\rho}, \tag{7}$$

where

$$N(k_y,\omega)=\frac{1}{Vk_BT}\mathcal{L}\langle P_{xy}(k_y,t)P_{xy}(k_y,0)\rangle \tag{8}$$

and $\mathcal{L}[\cdots]$ denotes the complex Laplace transform (one-sided Fourier transform) $\mathcal{L}[f(t)]=\int_0^\infty f(t)e^{-i\omega t}dt$. In the zero wave-vector limit, if the fluid can be assumed to be isotropic, the viscosity can be expressed as an orientational average over the elements of the autocorrelation function of the symmetric traceless stress tensor as

$$\eta=\frac{V}{10k_BT}\int_0^\infty dt\langle\overset{\circ s}{\mathbf{P}}(t):\overset{\circ s}{\mathbf{P}}(0)\rangle. \tag{9}$$

Equilibrium molecular dynamics simulations were performed on a system of particles interacting with the Weeks-Chandler-Andersen (WCA) potential energy function (a truncated and shifted form of the Lennard-Jones interaction) [9] at the temperatures and densities given in Table I with a time step of 0.004 reduced units. The transverse momentum density and stress autocorrelation functions were computed at wave vectors $k_n{=}2\pi n/L$ where $n{=}0$, 2, 4, 6, 8, 10, 12, 14, 16, 18, and 20 and $L{=}(N/\rho)^{1/3}$. The number of particles was $N{=}2048$ for all systems except the highest density for each temperature, for which $N{=}2916$, so as to keep the range of wave vectors roughly equal for all densities. After equilibration, a total of 2×10^7 time steps were used to compute the correlation functions at each state point by ensemble averaging 20 runs, each of length 1×10^6 steps, starting from independently equilibrated initial states. The transverse momentum density autocorrelation functions were computed at delay time intervals of 0.004 for 5000 delay time values and the stress autocorrelation functions were computed at 2500 delay time values, giving total delay times of 20 and 10 reduced time units, respectively. The correlation functions were then Laplace transformed with respect to time using Filon's rule [10], and the wave-vector and frequency dependent viscosities were calculated using Eqs. (3) and (7). Equation (3) was used to obtain the wave-vector dependent viscosity for nonzero wave vector and Eq. (7) was used to obtain the zero wave-vector viscosity, both at zero frequency.

TABLE I. Zero frequency, zero wave-vector shear viscosity, and fitted parameter values for Eqs. (24) and (26) at different state points.

	T_0=0.726				T_0=0.765			
ρ_0	0.374	0.438	0.485	0.698	0.375	0.450	0.480	0.685
η_0	0.274	0.340	0.397	0.971	0.273	0.354	0.390	0.929
A	0.417	0.498	0.406	0.628	0.440	0.507	0.399	0.492
σ_1	1.166	1.445	1.616	2.180	1.376	1.615	1.604	1.929
σ_2	4.587	4.674	4.892	4.442	4.750	4.762	4.879	4.497
α	0.234	0.160	0.131	0.048	0.180	0.126	0.131	0.080
β	1.547	1.753	1.805	2.438	1.662	1.886	1.808	2.142

B. Nonequilibrium molecular dynamics

The sinusoidal transverse force (STF) method is a nonequilibrium molecular dynamics technique for directly probing the response of a system to nonzero wave-vector velocity gradients [11]. In the STF method, a time-independent, spatially sinusoidal external field is applied to the system in order to induce a spatially varying but time independent stress. From the stress response, the wave-vector dependent viscosity can be obtained. This provides us with an independent set of results that can be used to verify the results of the equilibrium time correlation function analysis, and it can also provide us with an indication of the range of validity of the assumption of a linear constitutive equation. The details of the implementation of the STF method have been described in detail earlier [2,11,12] and we will here only give a brief outline of the method. An unconfined fluid is subjected to an external sinusoidal force field, $F_x(y)$, in the x direction given by

$$F_x(y) = F_0 \sin(k_n y), \tag{10}$$

where F_0 is the force field amplitude, $k_n = 2\pi n/L_y$ is the wave vector of the excitation, L_y is the length of the simulation box in the y direction, and the integer $n=1,2,\ldots$ is varied to control the wave vector of the external force field. In the limit of zero force field amplitude the streaming velocity obtained by solving the Navier-Stokes equations with the external force given by Eq. (10) takes the form $u_x(y) = \tilde{u}(k_n)\sin(k_n y)$. For larger amplitudes, the linear constitutive equation is no longer valid, and it is found that more terms are needed in the Fourier series representation of $u_x(y)$. Therefore we will write the streaming velocity, the density, and the temperature as a Fourier sine series or Fourier cosine series:

$$u_x(y) = \sum_{m=n}^{N} \tilde{u}_x(k_m)\sin(k_m y), \tag{11}$$

$$\rho(y) = \rho_0 + \sum_{m=n}^{N} \tilde{\rho}(k_{2m})\cos(k_{2m} y), \tag{12}$$

$$T(y) = T_0 + \sum_{m=n}^{N} \tilde{T}(k_{2m})\cos(k_{2m} y), \tag{13}$$

where the number of terms is arbitrary, i.e., we allow any higher order modes to be excited in order to keep the treatment as general as possible. $\tilde{u}_x(k_m)$, $\tilde{\rho}(k_{2m})$, and $\tilde{T}(k_{2m})$ are the Fourier coefficients in the three different series. Notice that the density and the temperature are expanded in even terms due to symmetry considerations [12]. The pressure tensor element $P_{xy}(y)$ can be evaluated via the momentum conservation equation [13]:

$$\begin{aligned} P_{xy}(y) &= \int F_x(y)\rho(y)dy \\ &= F_0 \int \sin(k_n y)\left[\rho_0 + \sum_{m=n}^{N} \tilde{\rho}(k_{2m})\cos(k_{2m} y)\right]dy \\ &= -\frac{F_0\rho_0}{k_n}\cos(k_n y) \\ &\quad + F_0 \sum_{m=n}^{N} \tilde{\rho}(k_{2m}) \int \sin(k_n y)\cos(k_{2m} y)dy, \end{aligned} \tag{14}$$

where we have assumed that the series converges uniformly to the function it represents. The integral is evaluated to

$$\begin{aligned} &\int \sin(k_n y)\cos(k_{2m} y)dy \\ &\quad = -\frac{\cos[(k_n - k_{2m})y]}{2(k_n - k_{2m})} - \frac{\cos[(k_n + k_{2m})y]}{2(k_n + k_{2m})}. \end{aligned} \tag{15}$$

Substituting Eq. (15) into Eq. (14) may not be of considerable help since the cosine terms are mixed. However, expanding the series and doing a bit of bookkeeping leads to the following expression for the stress:

$$\begin{aligned} P_{xy}(y) &= \frac{[\tilde{\rho}(k_{2n}) - 2\rho_0]F_0}{2k_n}\cos(k_n y) \\ &\quad + F_0 \sum_{m=n+1}^{N-n} \frac{\tilde{\rho}(k_{n+m}) - \tilde{\rho}(k_{m-n})}{2k_m}\cos(k_m y) \\ &\quad - F_0 \sum_{m=N-n+1}^{N+n} \frac{\tilde{\rho}(k_{m-n})}{2k_m}\cos(k_m y). \end{aligned} \tag{16}$$

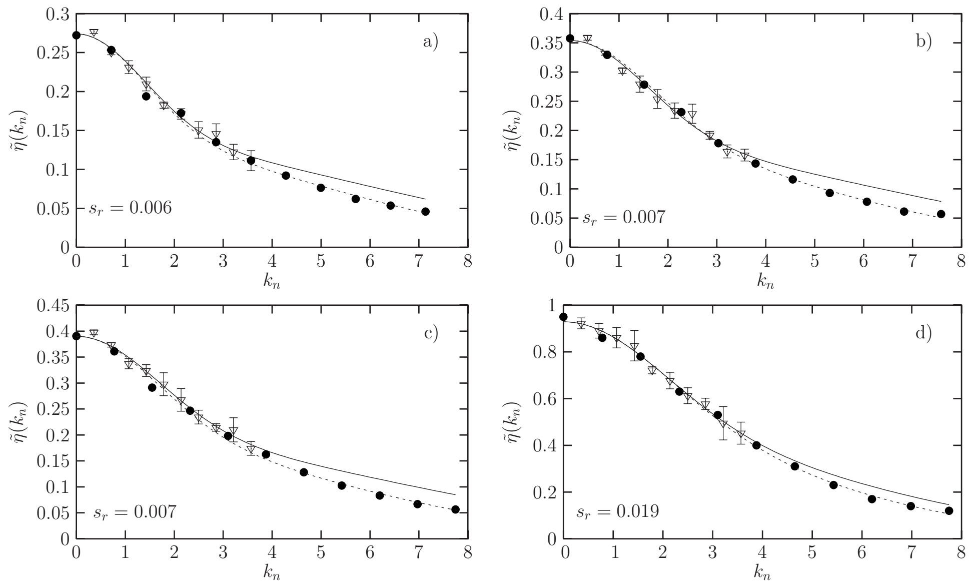

FIG. 1. $\tilde{\eta}(k_n)$ versus k_n for different densities and T_0=0.765. (a) ρ_0=0.375, (b) ρ_0=0.450, (c) ρ_0=0.480, and (d) ρ_0=0.685. The broken lines are the best fits of Eq. (24) to the EMD data (filled circles) and the full line the best fit to the NEMD data (triangles). The fits of the NEMD data are extrapolated for comparison. s_r is the standard deviation of the residuals.

This means that we can write the pressure tensor element as a Fourier cosine series:

$$P_{xy}(y) = \sum_{m=n}^{N} \tilde{P}_{xy}(k_m)\cos(k_m y), \tag{17}$$

where the Fourier coefficients are given by Eq. (16). Since the strain rate is here the only nonzero component of the velocity gradient tensor, $\dot{\gamma}(y)=\partial u_x/\partial y$, it is written as

$$\dot{\gamma}(y) = \sum_{m=n}^{N} \tilde{\dot{\gamma}}(k_m)\cos(k_m y) \tag{18}$$

with $\tilde{\dot{\gamma}}(k_m)=k_m\tilde{u}_x(k_m)$. From the linear constitutive equation and the convolution theorem we obtain the wave-vector dependent viscosity [2,14]:

$$\tilde{\eta}(k_m) = -\frac{\tilde{P}_{xy}(k_m)}{\tilde{\dot{\gamma}}(k_m)}. \tag{19}$$

The external force field applied here is sufficiently small such that higher order modes in the streaming velocity and density profiles are not excited. This means that in the limit of zero strain rate the system is homogeneous and only the first term in Eq. (18) is nonzero, i.e.,

$$\tilde{\eta}(k_n) = -\lim_{\dot{\gamma}\to 0} \frac{\rho_0 F_0}{k_n^2 \tilde{u}_x(k_n)}. \tag{20}$$

Recall that k_n is the wave vector of the external field, see Eq. (10).

The simulation box contains 1700 WCA particles and the length in the y direction is L_y=17.61 in all simulations. The x and z dimensions are then changed to obtain the desired density ρ_0 of the fluid. The system has periodic boundaries in all directions. For each state point, (T_0,ρ_0), we perform ten simulations each with a different external sinusoidal force field having wave vector $k_n=2\pi n/L_y$ where $n=1,\ldots,10$. For each wave vector four simulations with different external field amplitudes, F_0=0.05, 0.1, 0.15, and 0.2, are used in order to extrapolate to zero strain rate. The sample average of five such extrapolations is presented and the error estimate is given as half the maximum difference.

The external force field will generate heat in the system and the thermostated equations of motion for the ith particle in the STF simulations are given by [12]

$$\dot{\mathbf{r}}_i = \frac{\mathbf{p}_i}{m}, \quad \dot{\mathbf{p}}_i = \mathbf{F}_i + \mathbf{i}F_x(y) - \zeta[\mathbf{p}_i - m\mathbf{i}u_x(y_i)], \tag{21}$$

where the thermostating multiplier is

$$\zeta = \alpha_0 + \frac{1}{\rho(y_i)}\sum_{m=n}^{N} \alpha_m \cos(k_{2m} y_i), \tag{22}$$

$\mathbf{r}_i$ is the position, $\mathbf{p}_i$ is the particle laboratory momentum and $\mathbf{F}_i$ is the force acting on particle i due to the interactions with other particles. Equation (22) is based on Gauss' principle of least constraint and fixes the zero wave-vector components to the desired zero wave-vector temperature T_0 and all other temperature modes to zero. The dynamics of the multipliers can be obtained using a simple Nosé-Hoover feedback [12]:

$$\dot{\alpha}_0 = \frac{T - T_0}{Q_0} \quad \text{and} \quad \dot{\alpha}_m = \frac{\tilde{T}(k_{2m})}{Q_m}, \tag{23}$$

where $Q_0, Q_n, \ldots, Q_N$ are the Nosé-Hoover coupling strengths and are set to 10 in all simulations and $\tilde{T}(k_{2m})$ are the Fourier coefficients given in Eq. (13). These coefficients are found at each time step by a linear fit of the temperature data, obtained applying the method described in Ref. [3], to Eq. (13) using $N=n+5$. Equivalently, at each time step the Fourier coefficients in Eqs. (11) and (12) are evaluated by fitting them to density and streaming velocity data.

III. RESULTS AND DISCUSSION

In Fig. 1, $\tilde{\eta}(k_n)$ for T_0=0.765 and ρ_0=0.375, 0.450, 0.480, and 0.685 are displayed. It can be seen that the EMD and the

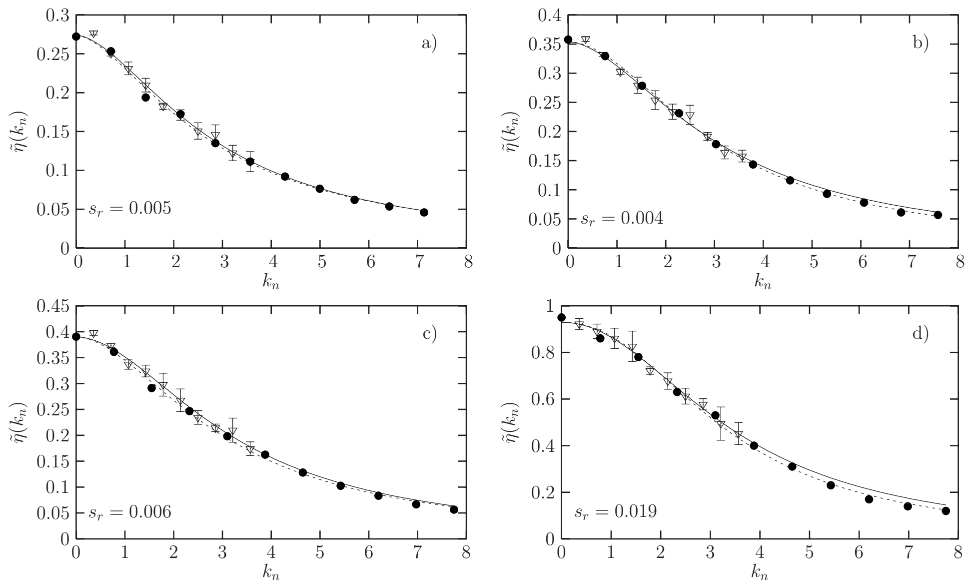

FIG. 2. Same as in Fig. 1, but where the data are fitted to Eq. (26).

NEMD results coincide within the statistical error. The data have unsuccessfully been fitted to numerous one parameter functional forms and we therefore turn to functions having two or three fitting parameters. In Fig. 1 the best fits of the data to a two term Gaussian function

$$\tilde{\eta}_G(k_n) = \eta_0\left(A e^{-k_n^2/2\sigma_1^2} + (1-A) e^{-k_n^2/2\sigma_2^2}\right), \quad A,\sigma_1,\sigma_2 \in \mathbb{R}_+ \tag{24}$$

are also included. In order to measure the magnitude of the residuals we use the residual standard deviation defined as

$$s_r = \sqrt{\frac{\sum_{n=1}^{N_s} r^2}{N_s - N_p}}, \tag{25}$$

where N_s is the number of data points, N_p is the number of fitting parameters, and r is the residual. The average residual standard deviation of the EMD and NEMD simulations are also shown in each figure. In Fig. 1 we have used η_0, σ_1, σ_2, and A as fitting parameters using the value of η_0 obtained from the EMD as the initial value for the zero frequency viscosity in the iterative curve fitting procedure. This then gives an accurate estimate of η_0. This value is then kept fixed allowing σ_1, σ_2, and A to be fitting parameters. In Table I we have listed all η_0 for every state point used. The fits of the NEMD data in Fig. 1 are extrapolated to higher wave vectors for comparison with the EMD data, and it is observed that the fit does not extrapolate well. To this end we have fitted the data to a Lorentzian type functional form:

$$\tilde{\eta}_L(k_n) = \frac{\eta_0}{1 + \alpha |k_n|^{\beta}}, \quad \alpha,\beta \in \mathbb{R}_+. \tag{26}$$

Figure 2 shows the same data as in Fig. 1, but where the data are fitted to Eq. (26). While there exists little difference in the residuals, the Lorentzian type functional form extrapolates to high values of wave vector better than the Gaussian form.

In order to compare the kernels for the different state points, the normalized EMD data are plotted in Fig. 3 for ρ=0.375, 0.450, and 0.685. Also shown is the best fits of Eq. (26). We see that for lower densities the kernel is, relatively, more flat for small wave numbers. However, for $k_n > 5$ the different kernels show similar behavior and the limiting behavior is the same.

The parameters in the two functional forms are functions of temperature and density. The density dependencies of σ_1, σ_2, and A in Eq. (24) are shown in Fig. 4. From this figure it is seen that σ_1 follows a power law and σ_2 and A are almost constant within the statistical error with an average value of $\sigma_2 \approx 4.7$ and $A \approx 0.5$. The parameter values used are the average of the values obtained from the EMD and NEMD data. The fact that $A \approx 0.5$ shows that the two terms in Eq. (24) are equally weighted and it can be written as a two parameter function:

$$\tilde{\eta}_G(k_n) = \frac{\eta_0}{2}\left(e^{-k_n^2/2\sigma_1^2} + e^{-k_n^2/2\sigma_2^2}\right). \tag{27}$$

Figure 5 suggests that α is an exponentially decreasing function of density, whereas β shows a simple linear increase with increasing density. That is

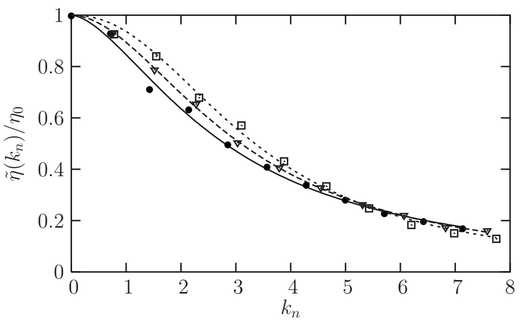

FIG. 3. Normalized EMD kernel data for ρ=0.375 (filled circles), 0.450 (triangles), and 0.685 (squares). The lines represent the best fits of Eq. (26) to the data.

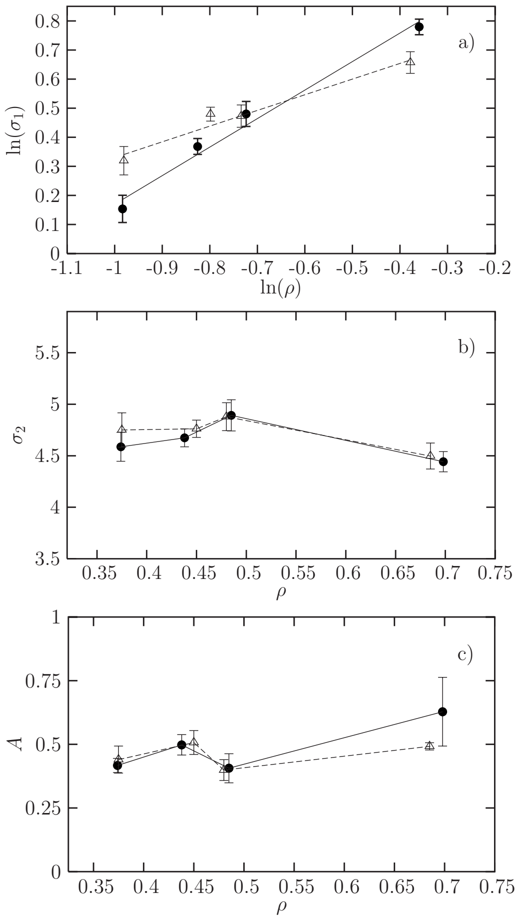

FIG. 4. Density dependence of σ_1, σ_2, and A. (a) $\ln(\sigma_1)$ as a function of $\ln(\rho)$. The fit for $T=0.765$ (triangles): $\ln(\sigma_1)=0.54\ln(\rho)+0.87$ (broken line) and for $T=0.726$ (filled circles): $\ln(\sigma_1)=0.98\ln(\rho)+0.15$ (full line). (b) σ_2 as a function of ρ. For $T=0.765$ (triangles): $\sigma_2=4.72\pm0.16$ and for $T=0.726$ (filled circles): $\sigma_2=4.65\pm0.19$. (c) A as a function of ρ. For $T=0.765$ (triangles): $A=0.46\pm0.05$ and for $T=0.726$ (filled circles) $A=0.49\pm0.10$. In (b) and (c) the lines serve as a guide to the eye. The error bars symbolize the estimated parameter standard deviation given in Ref. [22].

$$\sigma_1(\rho) \approx a_1\rho^{b_1}, \quad \sigma_2(\rho) \approx \sigma_2 \tag{28}$$

and

$$\alpha(\rho) \approx a_2 e^{-b_2\rho}, \quad \beta(\rho) \approx a_3\rho + b_3, \tag{29}$$

where a_n and b_n $(n=1,2,3)$ are functions of the temperature. See also the figure captions in Figs. 4 and 5. It is important to note that even though the temperature has a great impact on the parameters, the resulting kernels vary only slightly with the two temperatures chosen here. The fitted parameter values for the different state points are all listed in Table I.

It is possible to compare our results for the wave-vector dependent viscosity with the results previously obtained by Alley and Alder [7] for a hard sphere fluid. For this purpose, we must first find the approximate hard sphere diameter of our WCA atoms. Using the approximate formula for the Barker-Henderson equivalent hard sphere diameter given by Verlet and Weis [15], we find $d_{BH}=1.0266$ at $T=0.726$. A similar calculation of the equivalent hard sphere diameter using the WCA criterion [15] gives slightly density dependent values of 1.0269, 1.0267, 1.0264, and 1.0249 at densities of 0.374, 0.438, 0.485, and 0.698, respectively. If the hard sphere packing fraction is calculated using the WCA hard sphere diameter, we find that at a density of 0.438, our packing fraction ($\phi=0.248$) matches almost identically the packing fraction of Alley and Alder's $V/V_0=3$, $\phi=0.247$ system. The two data sets are compared in Fig. 6 together with an extrapolated fit of Eq. (26) to our EMD data. This plot shows that despite the difference between the interaction potentials, our results are very close to those of Alley and Alder. This confirms the expectation that the hard sphere model is an excellent reference point for dense liquid properties that depend on the liquid structure.

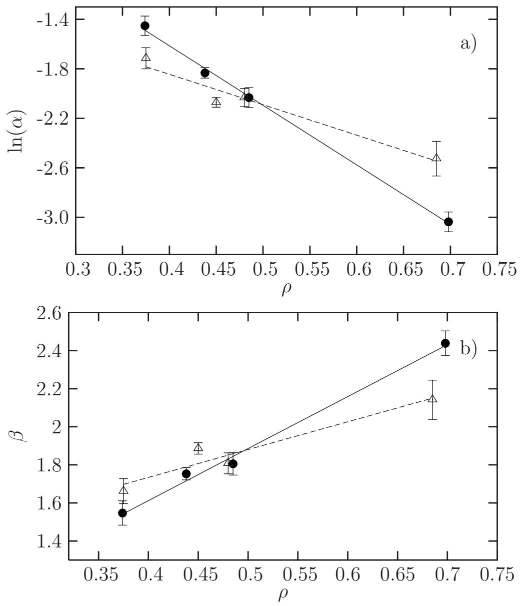

FIG. 5. Density dependence of α and β. (a) $\ln(\alpha)$ as a function of ρ. The fit for $T=0.765$ (triangles): $\ln(\alpha)=-2.46\rho-0.86$ (broken line) and for $T=0.726$ (filled circles): $\ln(\alpha)=-4.81\rho+0.31$ (full line). (b) β as a function of ρ. The fit for $T=0.765$ (triangles): $\beta=1.46\rho+1.15$ (broken line) and for $T=0.726$ (filled circles): $\beta=2.73\rho+0.52$ (full line).

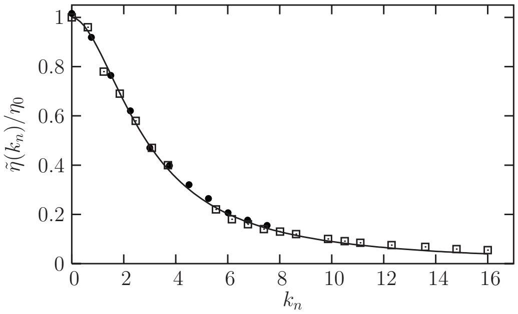

FIG. 6. Normalized EMD data for $\rho=0.438$ (filled circles) compared with data from Alley and Alder [7] (squares). Also shown is the best fit of Eq. (26) to our data (full line).

The two functions that we have used to represent our data, Eqs. (27) and (26), have fundamentally different behavior at small wave vector. The sum of Gaussians will always have a Taylor series expansion in the small wave-vector limit, but the Lorentzian type function will be nonanalytic for $k_n=0$, thereby rendering a Taylor expansion impossible. It is interesting to note in this context that a nonanalytic wave-vector dependence of the Navier-Stokes transport coefficients has been theoretically predicted by Keyes and Oppenheim [16]. On the other hand, the Burnett expansion predicts analytic behavior of the wave-vector dependent viscosity [16].

The best available theoretical predictions of the wave-vector dependent viscosity are based on mode-coupling theory [17,18]. While this theory improves on generalized Enskog theory [19], it does not achieve quantitative agreement with computer simulation data [7]. Furthermore, the main focus of the theory is the prediction of the momentum density autocorrelation function, which is found by an iterative numerical solution of a system of nonlinear equations. This does not result in analytical expressions for the correlation functions or the wave-vector dependent transport coefficients, which are the focus of the present study. The existing phenomenological memory-function treatments of generalized hydrodynamics also focus on the development of approximate expressions for the correlation functions rather than the spatially nonlocal transport coefficients. Therefore in the absence of guidance from theory, we have taken a pragmatic approach and simply proposed functional forms that provide a good fit to the data with a minimal number of free parameters, and that can easily be inverse transformed to the spatial domain.

We expect the kernel in the physical y space to be an even function since it is symmetric about the origin. This means that it can be found via an inverse Fourier cosine transform, $\mathcal{F}_c^{-1}[\cdots]$ of the kernel:

$$\mathcal{F}_c^{-1}[\tilde{\eta}(k)] = \eta(y) = \frac{1}{2\pi}\int_{-\infty}^{\infty}\tilde{\eta}(k)\cos(ky)dk. \qquad (30)$$

It can be shown that the inverse Fourier cosine transform of Eq. (27) exists [20] and it is even possible to obtain an analytical expression, namely

$$\eta_G(y) = \frac{\eta_0}{2\sqrt{2\pi}}[\sigma_1 e^{-(\sigma_1 y)^2/2} + \sigma_2 e^{-(\sigma_2 y)^2/2}]. \qquad (31)$$

While it can be shown that the function given in Eq. (26) fulfills the criteria for having an inverse Fourier transform $\eta_L(y)$ (i.e., the function is absolutely integrable and square integrable and the function and its derivative are piecewise continuous), the integral in Eq. (30) is not readily obtained analytically in the general case. However, the integral can be evaluated numerically by a simple Simpson or trapezoid method. We have also applied the Lado method [21] to improve the numerics, but without any measurable increase in the precision. Figure 7 shows the resulting kernels in y space for $T_0=0.765$ extracted from the two different functional forms, Eqs (26) and (27), and where the parameter fits have been used. For small y there exists a considerable difference between the kernels. This discrepancy decreases rapidly as can be seen in Fig. 8, where the difference between the two kernels, $\Delta\eta(y)=\eta_L(y)-\eta_G(y)$, is shown for $\rho=0.685$. At $y=0$ the difference is around 17% but becomes zero for $y \geqslant 1.0$.

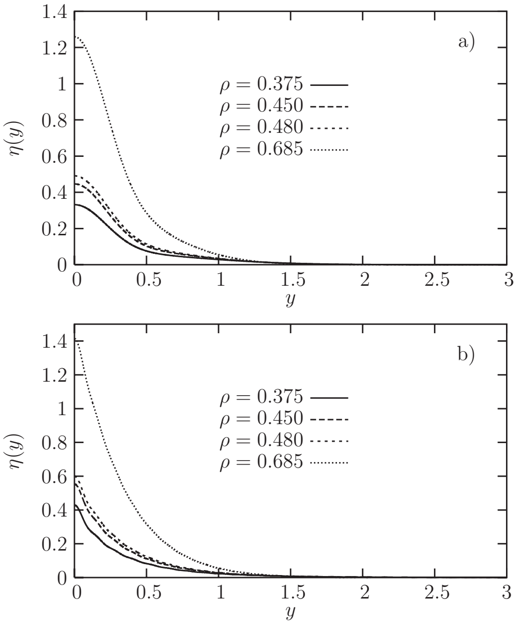

FIG. 7. Kernels in y space for $T_0=0.765$. (a) Kernels obtained from the Gaussian type functional form. (b) Kernels obtained from the Lorentzian type functional form.

It is important to stress that the local effective viscosity η_0 is obtained by integrating the nonlocal viscosity over y, i.e., for $\eta_G(y)$:

$$\int_{-\infty}^{\infty}\eta_G(y)dy = \frac{\eta_0}{2\sqrt{2\pi}}\int_{-\infty}^{\infty}[\sigma_1 e^{-(\sigma_1 y)^2/2} + \sigma_2 e^{-(\sigma_2 y)^2/2}]dy = \eta_0. \qquad (32)$$

Since an analytical expression for $\eta_L(y)$ does not exist we evaluate the integral numerically and we present numerical results from both functional forms in Table II. It is seen that error connected with the numerical integration is less than 2% comparing the zero frequency, zero wave-vector shear viscosities listed in Table II.

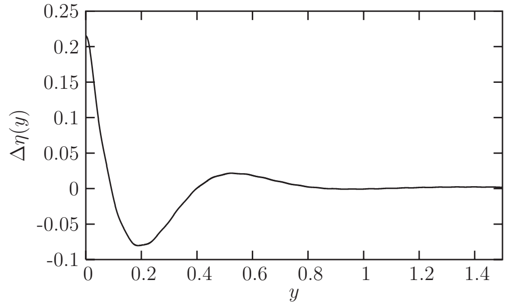

FIG. 8. Difference between the kernels in Fig. 7 for $\rho=0.685$ as a function of y. $\Delta\eta=\eta_L(y)-\eta_G(y)$.

TABLE II. Local effective viscosities evaluated numerically from the $\eta_G(y)$ and $\eta_L(y)$ using Eq. (32). $T_0=0.765$.

	$\eta_G(y)$				$\eta_L(y)$			
ρ_0	0.374	0.438	0.485	0.698	0.374	0.438	0.485	0.698
η_0	0.272	0.357	0.390	0.948	0.274	0.340	0.337	0.971

As mentioned above, it is not possible to analytically obtain the inverse Fourier transform for the general form of Eq. (26). However, for $\beta=2$ it reduces to a standard Lorentzian function, which has an inverse transform that is an exponentially decreasing function of the absolute value of y, i.e., the function features a cusp at $y=0$. This means that, in general, the derivative of the kernel in y space obtained through the Lorentzian type functional form does not exist for $y=0$ and a Taylor expansion of the real space viscosity kernel around the origin is not possible. In wave-vector space, of the two functional forms considered here, only the Gaussian form for the wave-vector dependent viscosity possesses a Taylor expansion about the zero wave vector. This is a useful property if the strain rate field only contains low spatial frequency components.

IV. CONCLUSION

We have computed the wave-vector dependent viscosity for a simple WCA model atomic fluid at a number of different state points. Our results agree almost precisely with previous results found by Alley and Alder [7] for hard sphere fluids. The results show that two relatively simple functional forms fit the data well—a sum of two Gaussians and a modified Lorentzian-type function with a variable wave-vector exponent in the denominator. The first of these has the advantage that an analytical expression can be found for the inverse Fourier transform to the spatial domain, whereas this is not generally possible for the second function. On the other hand, the Lorentzian-type function fits the data better at large values of the wave vector. The parameters of both functional forms has been shown to vary systematically with density, and simple expressions for their density dependence have been proposed.

The results show that in the spatial domain, the viscosity kernel has a width of roughly 2 to 3 molecular diameters. This means that the generalized viscosity must be used in order to correctly compute the velocity profile in systems where the strain rate varies significantly over a distance of 2 to 3 molecular diameters. In work currently in progress, we intend to use the viscosity kernel that we have obtained to predict the velocity profile of the same simple fluid undergoing planar Poiseuille flow in a channel of width less than 10 molecular diameters, where the strain rate has previously been shown to vary significantly.

Although our results have been obtained for an atomic fluid, we expect that similar methods could be used to study the nonlocal viscosity kernel for more complex molecular fluids. This nonlocal viscosity kernel could then be used to predict the velocity profile for nanoconfined flows of the corresponding molecular fluid. However, this is expected to be a far more complex problem than it is for a simple atomic fluid. In the atomic case, the viscosity kernel will vary with position due to the density variations in the confined fluid. For the molecular fluid, we must also consider the variation of the viscosity kernel with confinement-induced variations in molecular deformation, rotation, and alignment [23]. Investigations into these effects are currently underway.

ACKNOWLEDGMENT

The authors would like to thank the Australian Research Council for supporting this project as a part of a Discovery Grant.

[1] J. Boon and S. Yip, *Molecular Hydrodynamics* (McGraw-Hill, New York, 1980).

[2] D. J. Evans and G. P. Morriss, *Statistical Mechanics of Nonequilibrium Liquids* (Academic, New York, 1990).

[3] K. P. Travis, B. D. Todd, and D. J. Evans, Phys. Rev. E **55**, 4288 (1997).

[4] J. Zhang, B. D. Todd, and K. P. Travis, J. Chem. Phys. **121**, 10778 (2004).

[5] J. Zhang, B. D. Todd, and K. P. Travis, J. Chem. Phys. **122**, 219901 (2005).

[6] J. P. Hansen and I. R. McDonald, *Theory of Simple Liquids*, 2nd ed. (Academic, New York, 1986).

[7] W. E. Alley and B. J. Alder, Phys. Rev. A **27**, 3158 (1983).

[8] P. J. Cadusch, B. D. Todd, J. Zhang, and P. J. Daivis (unpublished).

[9] J. D. Weeks, D. Chander, and H. C. Andersen, J. Chem. Phys. **54**, 5237 (1971).

[10] M. P. Allen and D. J. Tildesley, *Computer Simulation of Liquids* (Oxford University, New York, 1989).

[11] E. M. Gosling, I. R. McDonald, and K. Singer, Mol. Phys. **26**, 1475 (1973).

[12] A. Baranyai, D. J. Evans, and P. J. Daivis, Phys. Rev. A **46**, 7593 (1992).

[13] B. D. Todd, D. J. Evans, and P. J. Daivis, Phys. Rev. E **52**, 1627 (1995).

[14] K. P. Travis, D. J. Searles, and D. J. Evans, Mol. Phys. **97**, 415 (1999).

[15] L. Verlet and J. J. Weis, Phys. Rev. A **5**, 939 (1972).

[16] T. Keyes and I. Oppenheim, Physica (Amsterdam) **70**, 100 (1973).

[17] E. Leutheusser, J. Phys. C **15**, 2801 (1982).

[18] E. Leutheusser, J. Phys. C **15**, 2827 (1982).

[19] S. Yip, W. E. Alley, and B. J. Alder, J. Stat. Phys. **27**, 201 (1982).

[20] A. Papoulis, *The Fourier Integral and Its Applications* (McGraw-Hill, New York, 1962).

[21] F. Lado, J. Comput. Phys. **8**, 417 (1971).

[22] Y. Bard, *Nonlinear Parameter Estimation* (Academic, New York, 1974).

[23] J. Zhang, J. S. Hansen, B. D. Todd, and P. J. Daivis, J. Chem. Phys. **126**, 144907 (2007).